DOI: 10.1002/hlca.201900065

FULL PAPER

HELVETICA chimica acta

Chiral Aggregates of Triphenylamine-Based Dyes for Depleting the Production of Hydrogen Peroxide in the Photochemical Water-Splitting Process

Beatrice Adelizzi,[a, b] Andreas T. Rösch,[a, b] Daan J. van Rijen,[a, b] R. Simone Martire,[a, b] Serkan Esiner,[a, b] Martin Lutz,[c] Anja R. A. Palmans,[a, b] and E. W. Meijer*[a, b]

[a] Laboratory of Macromolecular and Organic Chemistry, Eindhoven University of Technology, P.O. Box 513, NL-5600 MB Eindhoven, The Netherlands, e-mail: e.w.meijer@tue.nl

[b] Institute for Complex Molecular Systems, Eindhoven University of Technology, The Netherlands

[c] Crystal and Structural Chemistry, Bijvoet Center for Biomolecular Research, Utrecht University, Padualaan 8, NL-3584 CH Utrecht, The Netherlands

Dedicated to Prof. *François Diederich* for his outstanding contributions to science and for a lifelong friendship

Recent studies on water-splitting photoelectrochemical cells (PECs) have demonstrated the intriguing possibility of controlling the spin state in this chemical reaction to form H_2 and O_2 by exploiting the chirality of organic π-conjugated supramolecular polymers. Although this fascinating phenomenon has been disclosed, the chiral supramolecular materials reported thus far are not optimized for acting as efficient photosensitizer for dye-sensitized PECs. In this work we report on the design, synthesis, and characterization of chiral supramolecular aggregates based on C_3-symmetric triphenylamine-based dyes that are able to both absorb visible light and control the spin state of the process. Variable temperature-dependent spectroscopic measurements reveal the assembly process of the dyes and confirm the formation of chiral aggregates, both in solution as well as on solid supports. Photoelectrochemical measurements on TiO_2-based anodes validate the advantage of using chiral supramolecular aggregates as photosensitizer displaying higher photocurrent compared to achiral analogues. Moreover, fluorimetric tests for the quantification of the hydrogen peroxide produced, confirm the possibility of controlling the spin of the reaction exerting spin-selection with chiral supramolecular polymers. These results represent a further step towards the next-generation of organic-based water-splitting solar cells.

Keywords: dye-sensitized photoelectrochemical cells, water splitting, supramolecular chemistry, chirality, chiral induced spin selectivity.

Introduction

The production of H_2 and O_2 through photo- or electro-chemical processes has attracted many researches for the last thirty years.[1–5] Among the several devices studied for this aim, dye-sensitized photoelectrochemical cells (DS-PEC) offer an optimal compromise between efficiency, production-costs, and technical issues.[6] These devices closely resemble the structures used in n- and p-type dye-sensitized solar cells (DSSCs).[7] The DS-PECs are based on a high band-gap n- and/or p-type semiconductor functionalized with molecular sensitizers and are able to efficiently harvest the visible portion of the solar spectrum. However, the systems used are often affected by a significant overpotential and by the formation of peroxides and superoxide radicals as byproducts (especially for TiO_2 based photoanodes).[8–11] These byproducts, along with reducing the efficiency of the water-splitting process,

Supporting information for this article is available on the WWW under https://doi.org/10.1002/hlca.201900065

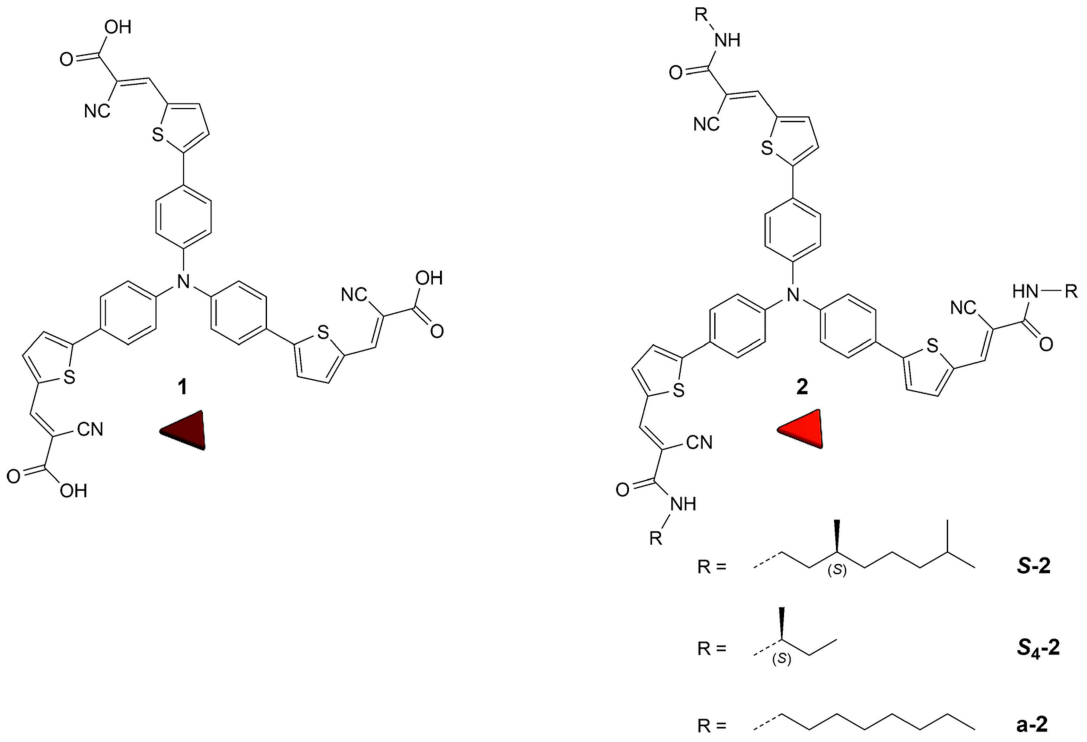

Figure 1. Molecular structure of triphenylamine-based D-π-A dyes **1** and **2**. The reference cyano-acetic **1** is used to synthesize the analogues bearing three cyano-acetamides with chiral (*S*)-3,7-dimethyloctyl chains, ***S*-2**, or three achiral *n*-octyl chains, **a-2**. An analogue with a short chiral chain ***S*$_4$-2** is synthesized for obtaining the crystal structure.

are known to poison and damage the surface, thereby reducing the device's lifetime.[8] Recently a possible solution to this problem was proposed by *Ron Naaman* and was demonstrated in collaboration with our group.[12,13] The functionalization of TiO_2 anodes with chiral supramolecular polymers that are able to act as spin filters – through an effect called chiral induced spin selectivity (CISS)[14] – demonstrated the possibility of simultaneously reducing the production of H_2O_2 and increasing the current.

This proof-of-concept highlighted the intriguing potential of controlling the spin of a reaction by exploiting the chirality of an organic film and created a promising route to next-generation water-splitting photoelectrochemical cells. The prototype cells used, however, were not optimized, especially with respect to the TiO_2 that was functionalized with chiral supramolecular polymers based on porphyrins or tripyridylamines. These anodes were neither designed to efficiently absorb visible light nor to adequately inject electrons into the TiO_2.[15,16] These issues evidenced the necessity of combining design rules required for obtaining helically aggregated supramolecular polymers with those for obtaining organic dyes that absorb visible light efficiently.

Organic dyes for the visible spectrum are often asymmetrically substituted conjugated molecules with a donor-π-bridge-acceptor structure (D-π-A).[17–19] However, bulkiness and asymmetry are qualities that may hamper the helical supramolecular organization. Therefore, coplanar aromatic systems combined with C_3-symmetrical amide functionalities bearing chiral chains are proposed to be ideal in achieving helical aggregation of organic dyes. This design for chirally ordered supramolecular polymers has been studied in detail and proved its importance in the formation of controlled 1D aggregates.[20,21]

Here, we report on the design, the synthesis, and the supramolecular characterization of new chiral supramolecular dyes and their application in DS-PECs. To merge the two prerequisites discussed above, we designed a C_3-symmetrical D-π-A dye which bears three carboxamides functionalized with chiral chains (*Figure 1*).

We selected a branched triphenylamine dye, similar to many dyes reported,[4][19][22] and directly related to the cyanoacetic acid analogue, **1**, which has been previously reported by *Shang et al.*[23] The small library of the cyanoacetamide derivatives, **2**, displays a triphenylamine core as donor unit, thiophene as π-

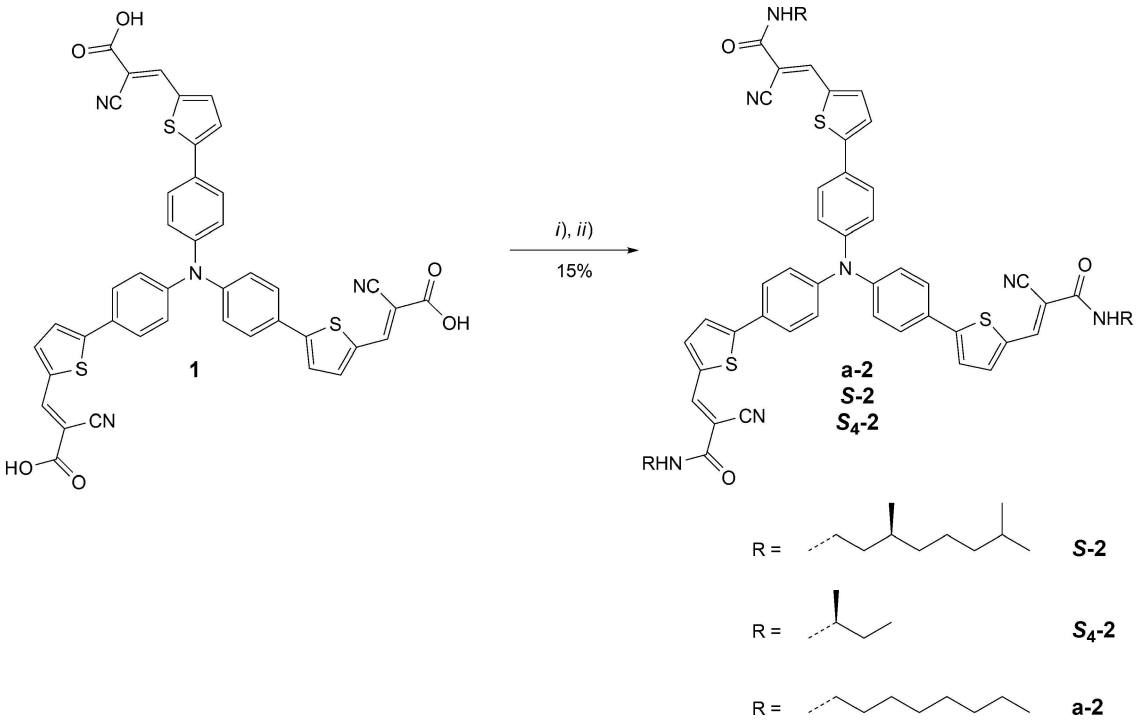

Scheme 1. Synthetic route from **1** to **2**. *i*) pentafluorophenyl trifluoroacetate, Et_3N, DMF, 0 °C to 20 °C, 4 h; *ii*) related primary amine, Et_3N, DMF, 20 °C, 18 h.

bridge, and a cyanoacetamide group which acts both as acceptor and as supramolecular unit. ***S*-2** comprises chiral (*S*)-3,7-dimethyloctyl side chains for relaying a bias in the helical sense of the assembly, while the achiral analogue, **a-2**, has *n*-octyl chains. In addition, an analogue molecule with short chiral chains, ***S*$_4$-2**, is designed to obtain a crystal structure.

The current study is ranging from molecular synthesis to device operation. It is inspired by the beautiful work of *François Diederich*, where he excels in combining original organic synthesis and comprehensive physical-organic characterization with fascinating applications. This study gives insight into how complex supramolecular monomers assemble and confirms the advantage of using a chiral light-harvesting layer in water-splitting devices.

Results and Discussion

Synthesis and Molecular Characterization

The target molecules ***S*-2**, **a-2**, and ***S*$_4$-2** were synthesized through amide coupling from **1** (*Scheme 1*). The synthesis of **1** was performed similarly to the procedure reported in literature (*Experimental Section*, *Scheme 2*).[23] The amide coupling was then performed through activation of **1** with pentafluorophenyl trifluoroacetate and consecutive substitution with the appropriate amine. SiO_2-gel chromatography and consecutive preparative thin layer chromatography (TLC) yielded the desired product in high purity. In contrast to **1**, which is a dark-red solid, ***S*-2**, **a-2**, and ***S*$_4$-2** are bright red-orange powders.

The molecules synthesized were characterized both in solution (^{1}H- and ^{13}C-NMR spectroscopy, mass spectrometry) and in bulk (IR spectroscopy, DSC, and polarized optical microscopy) to confirm the structures assigned (*Supporting Information*, *Figures S1* and *S2*). Subsequently, UV/Vis spectroscopic measurements in the molecularly dissolved state (DMSO, $c = 20$ μM; *Figure 2,a*) were performed to evaluate the absorption range of ***S*-2** and **a-2**.

Both the molecules display analogous spectra and molar extinction coefficients (ε) in line with ester analogues published previously.[24–28] ***S*-2** and **a-2** display a broad absorption between 300 and 600 nm with a maximum absorption at $\lambda = 474$ nm. This, in combination with ε of 6.9 10^4 cm^{-1} M^{-1}, demonstrates their suitability for harvesting visible light.

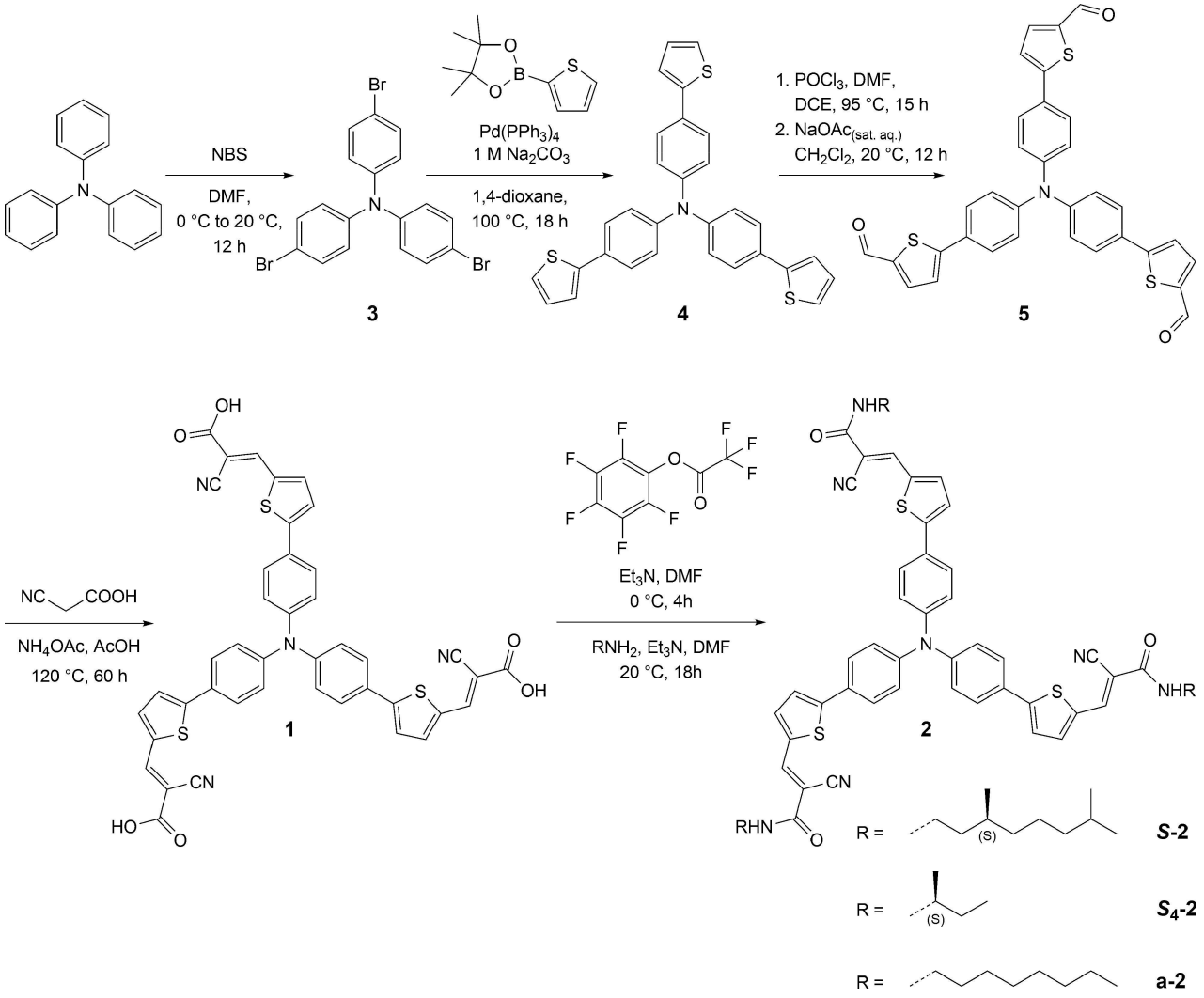

Scheme 2. Synthetic scheme followed for the synthesis of **2** derivatives.

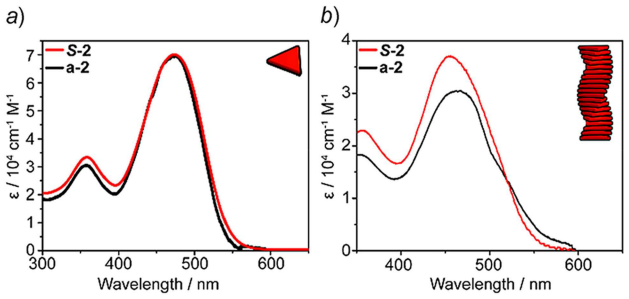

Figure 2. Molar extinction coefficient, ε, at 20 °C, for ***S*-2** (red lines) and **a-2** (black lines) in *a*) molecularly dissolved state in DMSO and *b*) in aggregated state in methylcyclohexane.

Supramolecular Polymerization

We then evaluated the aggregation of ***S*-2** and **a-2** in dilute solutions. In apolar methylcyclohexane (MCH), the supramolecular monomers tend to aggregate upon cooling. The aggregation processes can be followed by evaluating the variation of the optical features as a function of temperature. First, the aggregation was evaluated through UV/Vis spectroscopy on ***S*-2** and **a-2** in MCH at 20 °C. Both ***S*-2** and **a-2** display a reduced ε and a broader absorption spectrum, including a red-shifted shoulder at $\lambda =$ 515 nm, compared to measurements taken in DMSO (*Figure 2,b*). The difference in ε for **a-2** and ***S*-2** is probably due to an increased degree of aggregation of **a-2** due to its lower solubility in MCH. To further investigate the assembly and evaluate the ability of ***S*-**

2 to form chiral aggregates, variable temperature UV/Vis and circular dichroism (CD) measurements were performed by cooling ***S*-2** from 80 °C to 0 °C in MCH and acquiring spectra every 5 °C. Upon cooling, UV/Vis measurements display a decrease in intensity of the main absorption band at $\lambda = 448$ nm and the rise of a shoulder at $\lambda = 515$ nm (*Figure 3,a*). CD Spectroscopy reveals a bisignate *Cotton* effect with a negative extremum at $\lambda = 517$ nm (*Figure 3,b*), verifying that the chirality of periphery of ***S*-2** biases the helicity of the supramolecular polymers, resulting in the formation of chiral aggregates at room temperature. Analogous measurements on **a-2** display similar aggregation processes but the absence of CD signals, which as expected, indicates the formation of aggregates with no biased helicity (*Supporting Information*, *Figure S3*).

By following the evolution of UV and CD intensities as a function of temperature, it is possible to obtain insights into the mechanism of aggregation of ***S*-2**.[29] Three cooling curves varying the concentration of ***S*-2** were recorded ($\lambda = 522$, 80 °C to 0 °C, cooling rate: 15 °C h^{-1}; *Figure 3,d* and *3,e*). Interestingly, the cooling curves display slightly different starting temperatures in the UV and in the CD trace, which may be related to the formation of two different aggregates, the first of which does not display preferred helical organization, while the second shows preferred handedness. In addition, the shapes of both the cooling curves display a gradual increment (in absolute values) of the UV and CD intensities. Although the cooling curves in CD spectroscopy indicate a slightly cooperative nature of the polymerization, the curves can be fitted with an isodesmic model. This isodesmic character is probably due to a π-π driven aggregation, with a donor–acceptor contribution, rather than a cooperative supramolecular growth by triple hydrogen bonding.[30–32] This hypothesis, is also supported by IR spectroscopy in bulk (*Supporting Information, Figures S1* and *S2*). All results are consistent with the fact that, under analogous conditions, ***S*-2** assembles at a lower temperature than the well-known amide-based C_3-symmetric molecules that polymerize cooperatively through hydrogen bonding.[16,21]

Variable-temperature fluorescence measurements (***S*-2**, MCH, $c = 60$ μM) confirmed the formation of supramolecular polymers (*Figure 3,c*). At high temperature, molecularly dissolved ***S*-2** displays an emission band at $\lambda = 505$ nm with vibrational fine structures. This band first increases in intensity while cooling from 80 °C to 40 °C. Consecutively, the monomer

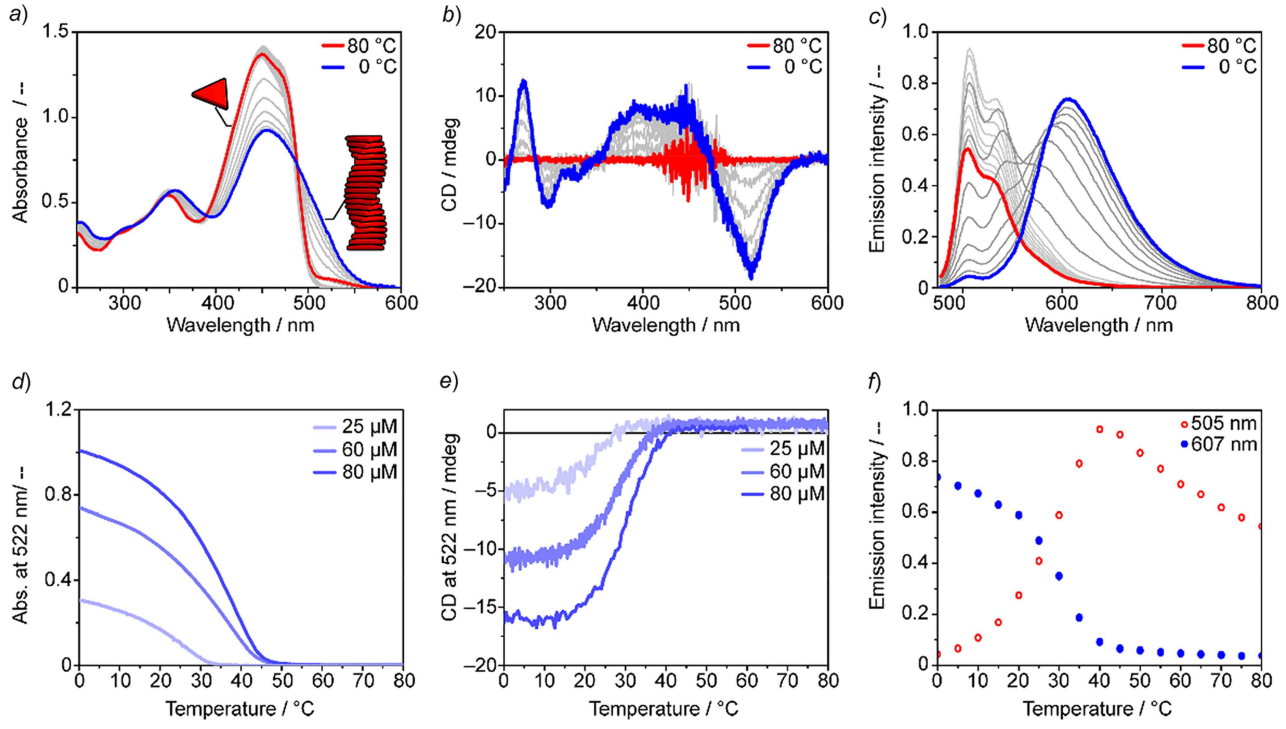

Figure 3. Variable temperature measurements of ***S*-2** in MCH measured from 80 °C (red lines) to 0 °C (blue line), intermediate spectra every 5 °C (grey lines), cooling rate: 15 °C h^{-1}. *a*) Absorbance spectra for $c = 25$ μM; *b*) CD spectra for $c = 60$ μM and *c*) emission spectra for $c = 60$ μM. *b*) Related cooling curves for *d*) absorbance, *e*) CD cooling curves ($\lambda = 522$ nm, cooling rate: 15 °C h^{-1}, $c = 25$ μM, 60 μM, and 80 μM), and *f*) emission cooling curves ($c = 60$ μM).

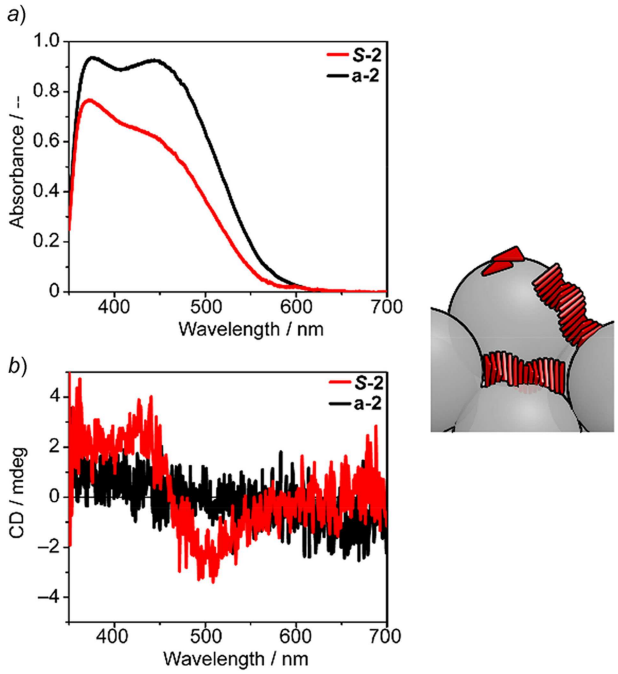

Figure 5. *a*) Absorbance and *b*) CD spectra of ***S*-2** (red lines) and **a-2** (black lines) on FTO/TiO_2 substrates. TiO_2 thickness 5 μm, ***S*-2** and **a-2** spincoated from $CHCl_3$, $c = 10$ mM, 1000 rpm, annealing 100 °C 30 min.

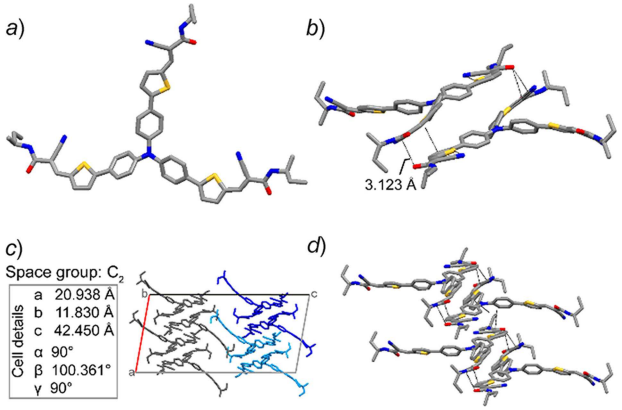

Figure 4. X-ray crystal structure of ***S*$_4$-2**. *a*) Molecular structure of one of the independent molecules in *b*) the asymmetric unit formed by two monomers. *c*) Crystalline packing in a unit cell projected along the b axis. Color coded by symmetry operation (blue, C_2 axis, light blue screw axis). *d*) Observed 1D arrangement in the crystal structure, seen along axis *b*. *a*), *b*), and *d*) Crystal structures color coded based on the atoms, C are grey, N blue, O red, S yellow. H not displayed.

emission band rapidly decreases in intensity while a broad band at $\lambda = 607$ nm grows reaching its maximum at 0 °C. The red-shifted band can be attributed to the aggregate state which is dominated by an intermolecular charge-transfer between donor and acceptor moieties. The cooling curves obtained by plotting the fluorescence maxima for the monomer (*Figure 3,f*, red open dots) and for the supramolecular aggregate (*Figure 3,f*, blue closed dots) display a starting temperature for aggregation coinciding with the one observed for the CD cooling curves (*Figure 3,f vs. Figure 3,d*). This observation indicates that the process which gives chirality to the supramolecular aggregates is the same that modifies the emission properties. The lack of an isosbestic point in the emission spectra is in agreement with the UV- and CD-data, indicating a complex aggregation behavior, instead of a simple nucleation-elongation mechanism.

To verify our hypothesis that donor-acceptor interactions and π-stacking are the driving interactions for the aggregation of ***S*-2**, we grew crystals of ***S*$_4$-2** suitable for single crystal X-ray diffraction. Needle-like crystals were afforded by vapor diffusion of diethyl ether into a concentrated $CHCl_3$ solution of ***S*$_4$-2**. The X-ray analyses confirmed the molecular structure of the monomer (*Figure 4,a*) which crystallizes in the non-centrosymmetric space group *C*2 with two independent molecules in the asymmetric unit (*Figure 4,b*) and approximately 8% of disordered solvent molecules in the unit cell volume (CCDC-1897910 contains the supplementary crystallographic data for this manuscript). The molecules lack molecular symmetry in the crystal structure (*Figure 4,a* and *4,b*) and due to the different conformations of the molecules, the non-crystallographic twofold axis between the independent molecules is only approximate (*Figure 4,b* and *4,c*). Interestingly, five of the six independent amide groups are connected by N–H···NC hydrogen bonds to form an infinite, two-dimensional network in the *b*, *c*-plane and no hydrogen bonds between amides are detected. Packing plots (*Figure 4,c* and *4,d*) display the 3D arrangements of the molecules. The high conjugation between the donating core and the cyanoacetamides renders the three branches of the molecule particularly planar, while the molecule itself shows a propeller geometry; well-known for triphenylamines.[33–35] This, in combination with the competing –CN groups, hampers the classic hydrogen bonding network of C_3 supramolecular polymers in the crystalline state.

We then tested the formation of chiral assemblies upon deposition of ***S*-2** both on glass (*Supporting Information*, *Figure S4,a*) and on TiO_2 surfaces (*Figure 5* and *Supporting Information*, *Figure S4,b*). TiO_2 Substrates functionalized with ***S*-2** or **a-2** (spin-coated from $CHCl_3$, $c = 10$ mM and annealing 100 °C, 30 min)

exhibit absorption spectra attributed to the aggregated state (*Figure 5,a* and *Supporting Information*, *Figure S4, top*). CD Spectroscopy on these surfaces confirms the presence of chiral aggregates for ***S*-2**, while **a-2** again does not form aggregates with any preferred chirality (*Figure 5,b* and *Supporting Information*, *Figure S4, bottom*). Remarkably, the structure of the chiral assemblies on TiO_2 matches well with the aggregates in solution as evidenced by CD spectroscopy (*Figure 5,b* and *Supporting Information*, *Figure S4,b*). These films were used in our devices.

Device Testing

Anatase TiO_2 photoanodes were fabricated following *Grätzel*'s procedure for DSSCs.[36] The electrodes were prepared on glass/FTO (fluorine doped tin oxide) substrates following the procedure reported for *Solaronix T/SP paste*® (commercially available TiO_2 paste, anatase 20 nm nanoparticles).[36] The as-prepared anodes were then characterized through X-Ray powder diffraction (XRD), ellipsometry and scanning electron microscopy (SEM; *Supporting Information*, *Figure S5*). To ensure the quality of the individual substrates, *I–V* curves were recorded for each photoanode, and a set of anodes with analogous electrochemical behavior was chosen for further experiments (*Supporting Information*, *Figure S6*). TiO_2 Substrates were used bare or functionalized with ***S*-2** or **a-2**, giving the respective electrodes ***S*-2/TiO$_2$** and **a-2/TiO$_2$**, (molecules deposited through spin-coating from $CHCl_3$ $c = 10$ mM and consequent annealing for 30 min at 100 °C).

Photoelectrochemical measurements were performed in a three-electrode cell, with Ag/AgCl (3 M KCl) as reference electrode and a Pt-plate as counter electrode (*Figure 6,a, left*, *Supporting Information*, *Figure S7*). A 0.1 M Na_2SO_4 (pH = 6.56) aqueous solution was used as the electrolyte (63 mL). Bare TiO_2 devices were tested both under dark conditions and under illumination (halogen lamp, 12 V, 50 W) to corroborate that in the dark no current is measured at 0 V *vs.* Ag/AgCl (*Supporting Information*, *Figure S8*). Next, functionalized and bare devices (***S*-2/TiO$_2$**, **a-2/TiO$_2$** and bare TiO_2) were tested by chronoamperometry measuring the magnitude of the current as a function of time (potential kept at 0 V *vs.* Ag/AgCl; *Figure 6,a*). For all samples, the experiments were performed four times to evaluate the reproducibility of the system. The related results are reported as means ± the associated standard deviation (*Figure 6,b*, lines and corresponding areas respectively). The measured current density, *J*, can be correlated with the number of water-splitting events and hence with the production of H_2 at the cathode and O_2 (and hydrogen peroxides) at the anode.[12] In line with studies reported previously,[12,13] these measurements confirm higher current for the chiral device compared to achiral analogues and bare TiO_2.

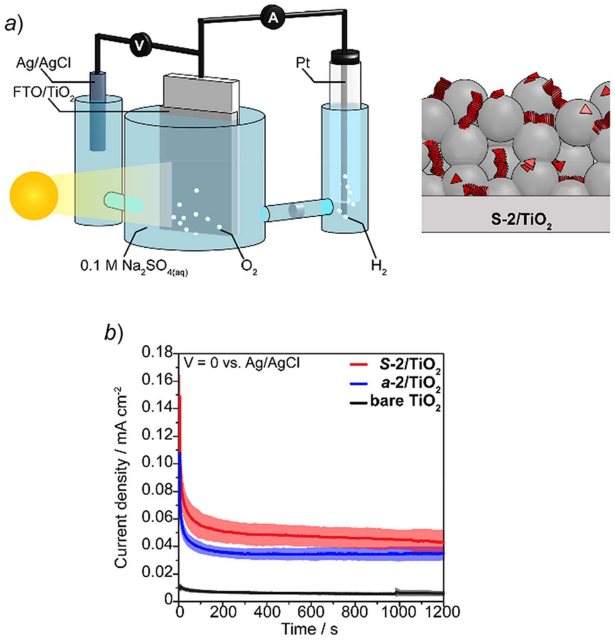

Figure 6. *a*) Schematic representation of the set up used (left) and of the TiO_2 anode functionalized with chiral supramolecular polymers (right). *b*) Current *vs.* time measurement of the devices under illumination and V = 0 *vs.* Ag/AgCl. Measurements reported as mean ± sd (lines ± solid background) ($n = 4$).

To evaluate the H_2O_2 production, after 20 minutes of constant irradiation and a potential kept at 0 V *vs.* Ag/AgCl, an aliquot was taken from the electrolyte solution and analyzed. A fluorimetric test based on horseradish peroxidase[37,38] was used to quantify the concentration of produced H_2O_2, based on a calibration curve (*Supporting Information*, *Figure S9*). The results show that ***S*-2/TiO$_2$** devices exhibit an average production of H_2O_2 that is 37% lower than that of **a-2/TiO$_2$** (*Table 1*). Remarkably, this happens although ***S*-2/TiO$_2$** displays higher current than **a-2/TiO$_2$** suggesting that the depletion of H_2O_2 byproducts correlates with a higher device efficiency. Lower [H_2O_2] were also detected for bare TiO_2. However, this is due to both the lower light absorption (due to the lack of photosensitizer) and the lower photocurrent. In order to appropriately compare the results of H_2O_2 production, we normalized the detected [H_2O_2], with the current

flowing through the device. To do so, we assumed the current measured at the 1000th sec (0 V *vs.* Ag/AgCl) as representative of the current in the steady state. We divided the $[H_2O_2]$ by this value (*Supporting Information*, *Tables S1* and *S2*). This normalization further highlights the effect of the homo-chirality. The ratio of $[H_2O_2]$ to current density, $[H_2O_2]\cdot J^{-1}$, for chiral devices is $(9.1\pm3.7)\,\mu M\ H_2O_2\ cm^2\,mA^{-1}$ which is nearly half of the value obtained for achiral devices. This result quantifies the effective gain of using chiral aggregates as photosensitizers and highlights the impact of the CISS effect on photoelectrochemical reactions.

Conclusions

After the first reports on using the CISS effect in the process of water-splitting, we add a new set of experiments to further strengthen the proposal made by *Ron Naaman*. Here, we report on the synthesis of chiral and achiral supramolecular dyes designed to both supramolecularly polymerize in a helical fashion and to harvest visible light. Absorption studies demonstrate the broad absorption range and suitability as visible sensitizers for both chiral and achiral analogues. The temperature-dependent spectroscopic measurements in apolar solutions verify the formation of chiral supramolecular aggregates through a proposed isodesmic mechanism. Fluorescence measurement and X-ray analysis indicate that the aggregation occurs mainly through donor-acceptor interactions.

Chronoamperometry measurements under light irradiation corroborate the higher photocurrent for devices with chiral dyes compared to the achiral equivalent. These results highlight the validity of the CISS effect in improving the cell's performances. The combination of the reduced H_2O_2 production with the increased photocurrent for **S-2/TiO$_2$** over **a-2/TiO$_2$** demonstrates the benefit of exploiting chiral dyes for photocatalytic applications and stresses the importance of controlling electrons' spins in chemical reactions involving multiple electrons. The encouraging results obtained in this study are, nevertheless, still far from a real exploitation in photoelectrochemical cells. However, we are confident that further optimization of the system will result in an effective use of the CISS effect in this important application.

Table 1. Hydrogen peroxide values for tested devices after 1200 sec of visible irradiation and V = 0 V *vs.* Ag/AgCl.

Device	Fluorescence intensity[a] [–]	$[H_2O_2]$[b] [μM]	J[c] [$\mu A\,cm^{-2}$]	$[H_2O_2]\cdot J^{-1}$[d] [$\mu M\,cm^2\,mA^{-1}$]
S-2/TiO$_2$	1191 ± 336	0.39 ± 0.12	45 ± 7	9.1 ± 3.7
a-2/TiO$_2$	1897 ± 871	0.62 ± 0.29	35 ± 5	17.5 ± 6.7
Bare TiO_2	440 ± 150	0.14 ± 0.05	6 ± 2	24.2 ± 10.4

[a] Fluorescence intensity detected with the fluorimetric test based on horseradish-peroxidase. [b] Concentration H_2O_2 based on calibration curve. [c] Current measured after 1000 sec, 0 V *vs.* Ag/AgCl. [d] Determined ratio of produced peroxide as a function of the photocurrent measured.

Experimental Section

Materials and Methods

All reagents were purchased from *Aldrich* and used as received, unless otherwise specified. Copper powder was acquired from *Aldrich* (< 425 μm, 99.5 % trace metals basis). All solvents were purchased from *Biosolve* and dry solvents were obtained using *MBraun* solvent purification system (*MB SPS-800*). Deuterated compounds were obtained from *Cambridge Isotopes Laboratories*. Reactions were followed by thin-layer chromatography (TLC) using *60-F254* silica gel plates from *Merck*.

Automated column chromatography was performed on a *Grace Reveleris X2* using *Reveleris Silica Flash Cartridges*. ^{1}H-NMR and ^{13}C-NMR measurements were conducted on a *Varian Mercury 200* MHz and/or a *Varian Gemini 400* MHz (100 MHz for ^{13}C). Proton chemical shifts are reported in ppm downfield from tetramethylsilane (TMS). Carbon chemical shifts are reported using the resonance of $CDCl_3$ as internal standard. MALDI-TOF-MS were acquired using a *PerSerptive Biosystem Voyager-DE PRO* spectrometer using α-cyano-4-hydroxycinnamic acid (CHCA) and 2-[(2*E*)-3-(4-tert-butylphenyl)-2-methylprop-2-enylidene] malononitrile (DCTB) as matrices. IR Spectra were recorded on a *Perkin–Elmer spectrum two* FT-IR spectrometer. Variable temperature IR spectra were recorded on a B*ruker Tensor 27 GladiATR* with temperature controller. Polarization optical microscopy (POM) measurements were done using a *Jenaval* polarization microscope equipped with a *Linkam THMS 600* heating device, with crossed polarizers. The thermal transitions were determined with DSC by using a *DSC Q2000 TA* under a nitrogen atmosphere with heating and cooling rates of 10 $K\,min^{-1}$.

For all spectroscopic measurements, cells with an optical path length of 1 cm were employed, and

spectroscopic-grade solvents were employed. Solutions were prepared by weighing the necessary amount of compound for the given concentration and dissolved with a weighted amount of solvent based on its density. The stock solutions were heated up, sonicated till complete dissolution and slowly cooled down to room temperature every time before use unless otherwise specified. All the spectroscopic measurements were performed with freshly prepared solutions (max. one week after the preparation of the stock solution).

UV/Vis and circular dichroism (CD) measurements were performed on a *Jasco J-815* spectropolarimeter, for which the sensitivity, time constants, and scan rates were chosen appropriately. Corresponding temperature-dependent measurements were performed with a *Jasco PFD-425S/15 Peltier*-type temperature controller with a temperature range of 263–393 K and adjustable temperature slope. In all experiments the linear dichroism was also measured and in all cases no linear dichroism was observed. Separate UV/Vis spectra were obtained from a *Perkin–Elmer* UV/Vis spectrometer *Lambda 40*. Fluorescence spectra were measured with *Jasco FMO-427S/15* fluorimeter implemented in the CD spectrometer.

The layer thicknesses were determined on a *Veeco Dektak150* profilometer after manually creating scratches with a sharp knife. Doctor blade coating of the TiO_2 layers was performed using an *Erichsen Model 360* 13 mm quadruple film applicator with gap heights of 30, 60, 90, and 120 μm. SEM and EDX was performed on a *FEI Nova600i SEM* with an *EDX* detector (136 eV resolution). Ellipsometry was performed using a *Sentech 805 SE* spectroscopic ellipsometer with a wavelength range 800–1700 nm. X-Ray Diffraction (XRD) measurements were performed on a *Rigaku Geigerex* powder diffractometer with *Bragg-Brentano* geometry, using copper radiation, wavelength 0.154 nm, at 40 kV and 30 mA. The samples were prepared on a glass substrate and measured from 5° till 80° 2θ with a step size of 0.02° and a dwell time of 15 seconds. The photoelectrochemical cell and the related measurements are described in a following section.

Single crystal X-ray diffraction analysis described in *Supporting Information*.

Synthetic Procedures

The cyanoacetic acid derivative, **1**, was synthesized adjusting a reported procedure[23] (*Scheme 2*), while the cyanoacetamide derivatives (**a-2**, ***S*-2**, ***S*$_4$-2**) were synthesized from **1** through activation with pentafluorophenyl trifluoroacetate.

Tris(4-bromophenyl)amine (=**4-Bromo-*N*,*N*-bis-(4-bromophenyl)aniline**; **3**). In a two-neck round bottom flask, triphenylamine (2.5 g, 10.0 mmol) was dissolved in anhydrous DMF (25 mL) under argon atmosphere. The solution was cooled to 0 °C by ice-water bath and NBS (5.2 g, 32.0 mmol) in DMF (10 mL) was added drop-wise under stirring. After the addition, the mixture was stirred for 4 h at room temperature. The mixture was then poured into water (400 mL), leading to the formation of a white precipitate. The precipitate was filtered and dried under reduced pressure. The crude product was recrystallized from heptane to afford pure **3** as a white solid (3.8 g, 77 %). ^{1}H-NMR (400 MHz, $CDCl_3$): 7.36–7.34 (*m*, 6 H); 6.93–6.91 (*m*, 6H). APCI-MS: 482.9 ($C_{18}H_{13}Br_3N^+$, $[M+H]^+$; calc. 481.9).

Tris[4-(2-thienyl)phenyl]amine (=**4-(Thiophen-2-yl)-*N*,*N*-bis[4-(thiophen-2-yl)phenyl]aniline**; **4**). In a three-neck round bottom flask, tris(4-bromophenyl) amine (**3**; 3 g, 6.2 mmol), thiophene-2-boronic acid pinacol ester (4.7 g, 22.4 mmol) and tetrakis(triphenylphosphine)palladium(0) (0.36 g, 0.31 mmol) were dissolved in dioxane (100 mL) under argon atmosphere. A 1 M Na_2CO_3 aqueous solution (30 mL) was introduced under stirring. The mixture was stirred and heated at 100 °C for 18 h, then cooled to room temperature and diluted with $CHCl_3$ (100 mL). The organic phase was then washed with water (150 mL), 1 M HCl (150 mL), and brine (150 mL), dried over anhydrous $MgSO_4$, filtered, and evaporated under vacuum. The crude product was purified through SiO_2 flash column chromatography (CH_2Cl_2/heptane 7:3 *v/v*) to afford **4** as a yellow solid (1.8 g, 57 %). ^{1}H-NMR (400 MHz, $CDCl_3$): 7.52 (*d*, J=8.7, 2 H); 7.26–7.22 (*m*, 2 H); 7.14 (*d*, J=8.6, 2 H); 7.07 (*dd*, J=5.1, 3.6, 1 H). MALDI-MS: 491.13 ($C_{30}H_{22}NS_3^+$, $[M+H]^+$; calc. 491.08).

Tris[4-(5-formyl-2-thienyl)phenyl]amine (=**5,5′,5″-[Nitrilotri(4,1-phenylene)]tri(thiophene-2-carbaldehyde)**; **5**). Tris[4-(2-thienyl)phenyl]amine (**4**) (800 mg, 1.63 mmol) was dissolved in 1,2-dichloroethane (50 mL) in a two-neck round bottom flask under argon. DMF (595 mg, 8.14 mmol) and $POCl_3$

(1.25 g, 8.14 mmol) were added dropwise and the solution was stirred and refluxed for 17 h. The mixture was then cooled to room temperature; CH_2Cl_2 (80 mL) and a saturated aqueous solution of sodium acetate (160 mL) were added. The mixture was then stirred at room temperature for 2 h. The organic phase was washed with water (3×150 mL), dried over anhydrous $MgSO_4$, filtered, and evaporated under vacuum, affording compound **5** as a yellow solid (1.04 g, 99%). IR: 2793, 1651, 1589, 1528, 1504, 1436, 1385, 1320, 1293, 1269, 1222, 1183, 1113, 1014, 960, 830, 800, 756, 736, 728, 697, 672, 648, 606, 594, 548, 499, 480, 547. ^{1}H-NMR (400 MHz, $CDCl_3$): 9.89 (*s*, 1 H); 7.74 (*d*, *J*=4.0, 1 H); 7.62 (*d*, *J*=8.8, 2 H); 7.36 (*d*, *J*=4.0, 1 H); 7.19 (*d*, *J*=8.7, 2 H). MALDI-MS: 575.12 ($C_{33}H_{21}NO_3S_3^+$, M^+; calc. 575.07).

3,3′,3″-[Nitrilotris(4,1-phenylene-5,2-thiophenediyl)]tris[2-cyano-2-propenoic acid] (=**3,3′,3″-{Nitrilotris[(4,1-phenylene)thiene-5,2-diyl]}tris(2-cyanoprop-2-enoic acid)**; **1**). In a two-neck round bottom flask, tris[4-(5-formyl-2-thienyl)phenyl]amine (**5**; 450 mg, 0.78 mmol), cyanoacetic acid (300 mg, 3.51 mmol), and ammonium acetate (42 mg, 0.55 mmol) were dissolved in glacial acetic acid (16 mL). The mixture was stirred and refluxed for 40 h under argon atmosphere. After completion, the mixture was cooled to room temperature, and the crude product was filtered and washed with $CHCl_3$ (about 50 mL). The crude product was purified by washing in $CHCl_3$ under reflux conditions for 15 h, to afford **1** as a dark red solid (406 mg, 67%). IR: 3175, 2824, 2218, 1738, 1690, 1565, 1493, 1416, 1321, 1258, 1185, 1063, 936, 799, 734, 683, 608, 582, 503. ^{1}H-NMR (400 MHz, (D_6)DMSO): 12.13 (*s*, 3 H); 8.49 (*s*, 3 H); 8.02 (*d*, *J*=4.1, 3 H); 7.79 (*d*, *J*=8.5, 6 H); 7.73 (*d*, *J*=4.0, 3 H); 7.21 (*d*, *J*=8.6, 6 H). ^{13}C-NMR (100 MHz, (D_6)DMSO): 164.13; 152.93; 147.58; 147.05; 142.11; 134.61; 128.24; 128.10; 125.18; 125.10; 117.03; 98.39. MALDI-MS: 776.09 ($C_{42}H_{24}N_4O_6S_3^+$, M^+; calc. 776.09).

*General Synthesis for (2*E*,2′*E*,2″*E*)-3,3′,3″-(5,5′,5″-(Nitrilotris(benzene-4,1-diyl))tris(thiophene-5,2-diyl))tris(2-cyano*-N*-alkylamides), i.e.,* **(2*E*,2′*E*,2″*E*)-3,3′,3″-{Nitrilotris[(4,1-phenylene)thiene-5,2-diyl]}tris(2-cyano-*N*-octylprop-2-enamide)** (**a-2**), **(2*E*,2′*E*,2″*E*)-3,3′,3″-{Nitrilotris[(4,1-phenylene)thiene-5,2-diyl]}tris{2-cyano-*N*-[(3*S*)-3,7-dimethyloctyl]prop-2-enamide}** (***S*-2**), and **(2*E*,2′*E*,2″*E*)-3,3′,3″-{Nitrilotris[(4,1-phenylene)thiene-5,2-diyl]}tris{*N*-[(2*S*)-butan-2-yl]-2-cyanoprop-2-enamide}** (***S*$_4$-2**). In a two-neck round bottom flask, compound 1 (300 mg, 0.39 mmol) and Et_3N (586 mg, 5.79 mmol, 1 ml) were dissolved in dry DMF (10 mL) under argon. The solution was cooled to 0 °C using an ice bath. In a second round bottom flask, pentafluorophenyl trifluoroacetate (487 mg, 1.74 mmol) was dissolved in dry DMF (1.5 mL) under argon atmosphere. This solution was added dropwise to the mixture containing 1, stirred at 0 °C for 1 h and then at room temperature for 4 h. Next, a solution of the appropriate alkylamine (1.74 mmol) was diluted in dry DMF (1.5 mL) under argon and then added to the mixture dropwise. The mixture was stirred for 40 h at room temperature. After completion, the mixture was diluted with $CHCl_3$ (150 mL), and the organic phase was washed with 1 N HCl (2×200 mL) and water (3×200 mL). The organic phase was dried over anhydrous $MgSO_4$, filtered, and evaporated under vacuum, affording a red oil. The crude product was precipitated from the red oil by pouring it in diethyl ether (120 mL) and filtered, affording a red solid. The crude product was first purified through SiO_2 flash column chromatography ($CHCl_3$/AcOEt 10:0.3 v/v) and then through preparative TLC ($CHCl_3$/AcOEt 10:0.3 v/v). After recrystallization from acetonitrile, the product was obtained pure as a red solid. The yield was estimated to be about 15%.

Data of **a-2**: IR: 3357, 3027, 2924, 2854, 2205, 1663, 1578, 1521, 1496, 1435, 1354, 1324, 1276, 1225, 1184, 1113, 1065, 940, 831, 802, 734, 734, 689, 609, 545, 504. ^{1}H-NMR (400 MHz, $CDCl_3$): 8.37 (*s*, 3 H); 7.68 (*d*, *J*=4.1, 3 H); 7.62 (*d*, *J*=8.7, 6 H); 7.35 (*d*, *J*=4.0, 3 H); 7.18 (*d*, *J*=8.7, 6 H); 6.24 (*t*, *J*=5.8, 3 H); 3.41 (*td*, *J*=7.2, 5.8, 6 H); 1.64–1.57 (*m*, 6 H); 1.43–1.21 (*m*, 30 H); 0.94–0.84 (*m*, 9 H). ^{13}C-NMR (100 MHz, $CDCl_3$): 160.5926; 154.42; 152.54; 147.48; 147.45; 144.41; 138.42; 135.02; 128.32; 127.68; 124.65; 123.74; 99.42; 99.15; 40.63; 31.78; 29.71; 29.48; 29.23; 29.17; 26.87; 22.64; 14.09. MALDI-MS: 1109.53 ($C_{66}H_{75}N_7O_3S_3^+$, M^+; calc. 1109.51). DSC (ramp: 10 K min^{-1}) Tg: 61.18 °C.

Data of ***S*-2**: IR: 3355, 3027, 2953, 2924, 2867, 2855, 2205, 1731, 1661, 1579, 1521, 1496, 1464, 1435, 1379, 1365, 1355, 1324, 1275, 1263, 1226, 1184, 1109, 1097, 1065, 1017, 959, 939, 830, 802, 753, 734, 689, 666, 627, 609, 599, 544, 505, 465. ^{1}H-NMR (400 MHz, $CDCl_3$): 8.36 (*s*, 3 H); 7.68 (*d*, *J*=4.0, 3 H); 7.62 (*d*, *J*=8.7, 6 H); 7.35 (*d*, *J*=4.0, 3 H); 7.18 (*d*, *J*=8.7, 6 H); 6.19 (*t*, *J*=5.7, 3 H); 3.44 (*dq*, *J*=8.2, 6.1, 6 H); 1.76–1.07 (*m*, 30 H); 0.94 (*d*, *J*=6.5, 9 H); 0.88 (*d*, *J*=0.7, 18 H). ^{13}C-NMR (100 MHz, $CDCl_3$): 171.15; 160.53; 152.52; 147.43; 144.36; 138.40; 135.00; 128.30; 127.66; 124.63; 123.72; 117.50; 99.15; 60.40; 39.21; 38.76; 37.09; 36.52; 30.70; 27.96; 24.62;

22.70; 22.60; 21.06; 19.50; 14.21. MALDI-MS: 1193.63 ($C_{72}H_{87}N_7O_3S_3^+$, $M]^+$; calc. 1193.60).

Data of ***S*$_4$-2**: IR: 3348, 2963, 2929, 2873, 2207, 1663, 1572, 1518, 1493, 1435, 1360, 1323, 1282, 1266, 1242, 1227, 1219, 1184, 1157, 1127, 1115, 1090, 1060, 1014, 939, 920, 875, 818, 801, 751, 734, 728, 687, 674, 665, 621, 602, 544, 510, 498, 452, 407. ^{1}H-NMR (400 MHz, $CDCl_3$): 8.37 (*s*, 3 H); 7.68 (*d*, $J=4.0$, 3 H); 7.63 (*d*, $J=8.9$, 6 H); 7.35 (*d*, $J=4.0$, 3 H); 7.18 (*d*, $J=9.0$, 6 H); 5.99 (*d*, $J=8.3$, 3 H); 4.08–3.99 (*m*, 3 H); 1.56 (*d*, $J=8.2$, 6 H); 1.25 (*td*, $J=8.0$, 6.3, 9 H); 0.96 (*t*, $J=7.4$, 9 H). ^{13}C-NMR (100 MHz, $CDCl_3$): 159.93; 152.48; 147.43; 144.41; 138.36; 135.03; 128.32; 127.66; 32 124.63; 123.72; 117.50; 99.33; 77.23; 65.86; 47.96; 29.60; 20.35; 15.28; 10.37.

Acknowledgements

The authors acknowledge Dr. *Chidambar Kulkarni* for the help with the TiO_2 substrates, *Ingeborg Schreur* for SEM. Would like to thank Dr. *Stefan Meskers*, Prof. Dr. *René Janssen*, and Prof. Dr. *Ron Naaman* and his group for fruitful discussions. We acknowledge funding from the Dutch Ministry of Education, Culture and Science (Gravity program 024.001.035).

Author Contribution

B. A. conceived the project and designed the experiments. *B. A.*, *A. T. R.*, *A. J. R.*, and *R. S. M.* performed the experiments. *B. A.*, *A. T. R.*, and *S. E.* analyzed the data. *M. L.* determined the crystal structure of ***S*$_4$-2**. *B. A.*, *A. T. R.*, *A. R. A. P.*, and *E. W. M.* wrote the manuscript. *A. R. A. P.* and *E. W. M.* supervised the research.

References

[1] S. Y. Reece, J. A. Hamel, K. Sung, T. D. Jarvi, A. J. Esswein, J. J. H. Pijpers, D. G. Nocera, 'Wireless Solar Water Splitting Using Silicon-Based Semiconductors and Earth-Abundant Catalysts', *Science* **2011**, *334*, 645–648.

[2] Y. Tachibana, L. Vayssieres, J. R. Durrant, 'Artificial Photosynthesis for Solar Water-Splitting', *Nat. Photonics* **2012**, *6*, 511–518.

[3] B. Gu, J. Kiwi, M. Grätzel, 'Photochemical Water Cleavage in Suspensions of Pt-Loaded Titania Particles with 0.7% Overall Light to Chemical Conversion Efficiency', in 'Hydrogen Systems', Eds. T. N. Veziroglu, Y. Zhu, D. Bao, Pergamon Press, Oxford, 1986, pp. 121–134.

[4] B. Cecconi, N. Manfredi, T. Montini, P. Fornasiero, A. Abbotto, 'Dye-Sensitized Solar Hydrogen Production: The Emerging Role of Metal-Free Organic Sensitizers', *Eur. J. Org. Chem.* **2016**, 5194–5215.

[5] H. B. Gray, 'Powering the Planet with Solar Fuel', *Nat. Chem.* **2009**, *1*, 7.

[6] X. Ding, Y. Gao, L. Ye, L. Zhang, L. Sun, 'Assembling Supramolecular Dye-Sensitized Photoelectrochemical Cells for Water Splitting' *ChemSusChem* **2015**, *8*, 3992–3995.

[7] M. K. Nazeeruddin, A. Kay, I. Rodicio, R. Humphry-Baker, E. Mueller, P. Liska, N. Vlachopoulos, M. Graetzel, 'Conversion of Light to Electricity by *cis*-X_2Bis(2,2′-bipyridyl-4,4′-dicarboxylate)ruthenium(II) Charge-Transfer Sensitizers (X=Cl^-, Br^-, I^-, CN^-, and SCN^-) on Nanocrystalline TiO_2 Electrodes', *J. Am. Chem. Soc.* **1993**, *115*, 6382–6390.

[8] J. A. Seabold, K.-S. Choi, 'Effect of a Cobalt-Based Oxygen Evolution Catalyst on the Stability and the Selectivity of Photo-Oxidation Reactions of a WO_3 Photoanode', *Chem. Mater.* **2011**, *23*, 1105–1112.

[9] J. Kiwi, M. Graetzel, 'Specific Analysis of Surface-Bound Peroxides Formed during Photoinduced Water Cleavage in Titanium Dioxide-Based Microheterogeneous Systems', *J. Mol. Catal.* **1987**, *39*, 63–70.

[10] E. Yesodharan, S. Yesodharan, M. Grätzel, 'Photolysis of Water with Supported Noble Metal Clusters, the Fate of Oxygen in Titania Based Water Cleavage Systems', *Solar Energy Mater.* **1984**, *10*, 287–302.

[11] O. C. Compton, F. E. Osterloh, 'Niobate Nanosheets as Catalysts for Photochemical Water Splitting into Hydrogen and Hydrogen Peroxide', *J. Phys. Chem. C* **2009**, *113*, 479–485.

[12] W. Mtangi, V. Kiran, C. Fontanesi, R. Naaman, 'Role of the Electron Spin Polarization in Water Splitting', *J. Phys. Chem. Lett.* **2015**, *6*, 4916–4922.

[13] W. Mtangi, F. Tassinari, K. Vankayala, A. Vargas Jentzsch, B. Adelizzi, A. R. A. Palmans, C. Fontanesi, E. W. Meijer, R. Naaman, 'Control of Electrons' Spin Eliminates Hydrogen Peroxide Formation during Water Splitting', *J. Am. Chem. Soc.* **2017**, *139*, 2794–2798.

[14] R. Naaman, D. H. Waldeck, 'Spintronics and Chirality: Spin Selectivity in Electron Transport Through Chiral Molecules', *Annu. Rev. Phys. Chem.* **2015**, *66*, 263–281.

[15] G. F. Moore, J. D. Blakemore, R. L. Milot, J. F. Hull, H. Song, L. Cai, C. A. Schmuttenmaer, R. H. Crabtree, G. W. Brudvig, 'A Visible Light Water-Splitting Cell with a Photoanode Formed by Codeposition of a High-Potential Porphyrin and an Iridium Water-Oxidation Catalyst', *Energy Environ. Sci.* **2011**, *4*, 2389–2392.

[16] B. Adelizzi, I. A. W. Filot, A. R. A. Palmans, E. W. Meijer, 'Unravelling the Pathway Complexity in Conformationally Flexible *N*-Centered Triarylamine Trisamides', *Chem. Eur. J.* **2017**, *23*, 6103–6110.

[17] B. E. Hardin, H. J. Snaith, M. D. McGehee, 'The Renaissance of Dye-Sensitized Solar Cells', *Nat. Photonics* **2012**, *6*, 162–169.

[18] H. Meier, Z.-S. Huang, D. Cao, 'Double D-π-A Branched Dyes – a New Class of Metal-Free Organic Dyes for Efficient Dye-Sensitized Solar Cells', *J. Mater. Chem. C* **2017**, *5*, 9828–9837.

[19] N. Manfredi, B. Cecconi, A. Abbotto, 'Multi-Branched Multi-Anchoring Metal-Free Dyes for Dye-Sensitized Solar Cells', *Eur. J. Org. Chem.* **2014**, 7069–7086.

[20] L. Brunsveld, A. P. H. J. Schenning, M. A. C. Broeren, H. M. Janssen, J. A. J. M. Vekemans, E. W. Meijer, 'Chiral Amplification in Columns of Self-Assembled N,N′,N″-Tris((*S*)-3,7-dimethyloctyl)benzene-1,3,5-tricarboxamide in Dilute Solution', *Chem. Lett.* **2000**, *29*, 292–293.

[21] P. J. M. Stals, J. C. Everts, R. de Bruijn, I. A. W. Filot, M. M. J. Smulders, R. Martín-Rapún, E. A. Pidko, T. F. A. de Greef, A. R. A. Palmans, E. W. Meijer, 'Dynamic Supramolecular Polymers Based on Benzene-1,3,5-tricarboxamides: The Influence of Amide Connectivity on Aggregate Stability and Amplification of Chirality', *Chem. Eur. J.* **2010**, *16*, 810–821.

[22] A. Mahmood, 'Triphenylamine Based Dyes for Dye Sensitized Solar Cells: A Review', *Sol. Energy* **2016**, *123*, 127–144.

[23] H. Shang, Y. Luo, X. Guo, X. Huang, X. Zhan, K. Jiang, Q. Meng, 'The Effect of Anchoring Group Number on the Performance of Dye-Sensitized Solar Cells', *Dyes Pigm.* **2010**, *87*, 249–256.

[24] H. J. Yun, N. T. Hai, C. J. Min, S. Thogiti, R. Cheruku, J. H. Kim, 'Influence of Diffusion Coefficient of Cobalt Redox Mediator Using Triphenylamine Dyes with Various Number of Anchoring Groups: Photovoltaic Performance of DSSCs', *Electrocatalysis* **2017**, *8*, 414–421.

[25] Y.-W. Kao, W.-H. Lee, R.-J. Jeng, C.-F. Huang, J. Y. Wu, R.-H. Lee, 'Peripheral Group Effects on the Photophysical and Photovoltaic Properties of Bulk-Heterojunction Type Solar Cells Based on Star-Shaped Conjugate Molecules with Triphenylamine Core', *Mater. Chem. Phys.* **2015**, *163*, 138–151.

[26] Y. H. Lee, H. J. Yun, S. K. Choi, Y. S. Yang, T. Park, K.-S. Ahn, T. Suresh, J. H. Kim, 'Triphenylamine-Based Tri-Anchoring Organic Dye with Enhanced Electron Lifetime and Long-Term Stability for Dye Sensitized Solar Cells', *Synth. Met.* **2016**, *217*, 248–255.

[27] W. Li, Q. Li, C. Duan, S. Liu, L. Ying, F. Huang, Y. Cao, 'Design and Synthesis of Star-Burst Triphenyamine-Based π-Conjugated Molecules', *Dyes Pigm.* **2015**, *113*, 1–7.

[28] G. Casalbore-Miceli, A. Degli Esposti, V. Fattori, G. Marconi, C. Sabatini, 'A Correlation between Electrochemical Properties and Geometrical Structure of Some Triarylamines Used as Hole Transporting Materials in Organic Electroluminescent Devices', *Phys. Chem. Chem. Phys.* **2004**, *6*, 3092–3096.

[29] T. F. A. De Greef, M. M. J. Smulders, M. Wolffs, A. P. H. J. Schenning, R. P. Sijbesma, E. W. Meijer, 'Supramolecular Polymerization', *Chem. Rev.* **2009**, *109*, 5687–5754.

[30] C. Kulkarni, E. W. Meijer, A. R. A. Palmans, 'Cooperativity Scale: A Structure-Mechanism Correlation in the Self-Assembly of Benzene-1,3,5-tricarboxamides', *Acc. Chem. Res.* **2017**, *50*, 1928–1936.

[31] T. Haino, A. Watanabe, T. Hirao, T. Ikeda, 'Supramolecular Polymerization Triggered by Molecular Recognition between Bisporphyrin and Trinitrofluorenone', *Angew. Chem. Int. Ed.* **2012**, *51*, 1473–1476.

[32] U. Mayerhöffer, F. Würthner, 'Halogen-Arene Interactions Assist in Self-Assembly of Dyes', *Angew. Chem. Int. Ed.* **2012**, *51*, 5615–5619.

[33] D. Lionetti, A. J. Medvecz, V. Ugrinova, M. Quiroz-Guzman, B. C. Noll, S. N. Brown, 'Redox-Active Tripodal Aminetris (aryloxide) Complexes of Titanium(IV)', *Inorg. Chem.* **2010**, *49*, 4687–4697.

[34] Q. Wang, Z. He, A. Wild, H. Wu, Y. Cao, U. S. Schubert, C.-H. Chui, W.-Y. Wong, 'Platinum-Acetylide Polymers with Higher Dimensionality for Organic Solar Cells', *Chem. Asian J.* **2011**, *6*, 1766–1777.

[35] V. Parthasarathy, S. Fery-Forgues, E. Campioli, G. Recher, F. Terenziani, M. Blanchard-Desce, 'Dipolar versus Octupolar Triphenylamine-Based Fluorescent Organic Nanoparticles as Brilliant One- and Two-Photon Emitters for (Bio) imaging', *Small* **2011**, *7*, 3219–3229.

[36] H. Choi, C. Baik, S. O. Kang, J. Ko, M.-S. Kang, M. K. Nazeeruddin, M. Grätzel, 'Highly Efficient and Thermally Stable Organic Sensitizers for Solvent-Free Dye-Sensitized Solar Cells', *Angew. Chem. Int. Ed.* **2008**, *47*, 327–330.

[37] Y. Sun, D. Zhang, M. Mao, Y. Lu, N. Jiao, 'Roles of p38 and JNK Protein Kinase Pathways Activated by Compound Cantharidin Capsules Containing Serum on Proliferation Inhibition and Apoptosis of Human Gastric Cancer Cell Line', *Exp. Ther. Med.* **2017**, *14*, 1809–1817.

[38] K. Zaitsu, Y. Ohkura, 'New Fluorogenic Substrates for Horseradish Peroxidase: Rapid and Sensitive Assays for Hydrogen Peroxide and the Peroxidase', *Anal. Biochem.* **1980**, *109*, 109–113.

Received February 24, 2019
Accepted March 22, 2019